Electrical characterization of a graphite-diamond-graphite junction fabricated by MeV carbon implantation

Electrical characterization of a graphite-diamond-graphite junction fabricated by MeV carbon implantation

S. Ditalia Tchernij[1,2], N. Skukan[3], F. Picollo[2,1], A. Battiato[1], V. Grilj[3], G. Amato[4], L. Boarino[4], E. Enrico[4], M. Jakšić[3], P. Olivero[1,2], J. Forneris[2,1,]*

[1]*Physics Department and "NIS " Inter-departmental Centre - University of Torino; via P. Giuria 1, 10125, Torino, Italy*
[2]*Istituto Nazionale di Fisica Nucleare (INFN), Sez. Torino, via P. Giuria 1, 10125, Torino, Italy*
[3]*Ruđer Bošković Institute, Bijenicka 54, P.O. Box 180, 10002 Zagreb, Croatia*
[4]*Istituto Nazionale di Ricerca Metrologica (INRiM); Strada delle Cacce 91, 10135 Torino, Italy*

** Corresponding author. Email:* forneris@to.infn.it

Abstract

The Deep Ion Beam Lithography technique has been extensively adopted in recent years for the fabrication of graphitic electrodes in bulk diamond with a wide range of technological applications. Particularly, it has been recently shown that a high current can be driven in devices consisting of micrometer-spaced sub-superficial graphitic electrodes. This effect has been exploited to stimulate electroluminescence from color centers placed in the active region of the device.
A deep understanding of the conduction mechanisms governing charge transport in micro-regions of defective diamond comprised between graphitic electrodes is necessary in order to fully exploit the functionality of these opto-electronic devices, as well as to assess the ion-beam-micromachining of diamond as a convenient technique for the fabrication of solid-state micro-devices.
In this work, a temperature-dependent characterization of the electrical properties of a sub-superficial graphite-diamond-graphite junction is presented and discussed. The ohmic behavior observed at low bias voltages is ascribed to a donor level with an activation energy of (0.217 ± 0.002) eV, a value compatible with previous reports on nitrogen-related defects. A transition to a high-current regime above a critical voltage V_C was also observed, and interpreted in terms of the Space-Charge-Limited Current model. The temperature-dependent measurements allowed to investigate the role of charge trapping in the charge injection mechanism of the junction. By fitting the temperature dependence in the high-current regime it was possible to determine the relevant trap level of the associated Poole-Frenkel mechanism, leading to a value of (0.278 ± 0.001) eV from the conduction band. The Poole-Frenkel conduction model in high-current regime enabled also a preliminary investigation in the effects of ion implantation on the modification of the dc dielectric constant of diamond.

Keywords
diamond, graphite , implantation, radiation induced effects, electrical properties characterization

Highlights

- fabrication of a sub-superficial graphite-diamond-graphite junction with a 6 MeV C microbeam
- temperature-dependent electrical characterization by means of current-voltage and current-temperature curves
- transition from low-current to high-current at a critical threshold voltage
- identification of the relevant energy levels for bulk electrical conduction as nitrogen-related defects
- determination of the dc dielectric constant in ion implanted diamond according to the Poole-Frenkel model

1. Introduction

In recent years, the progresses in the quality of diamond synthesis by chemical vapor deposition (CVD) has paved the way for the full exploitation of the extreme properties of this material in innovative and challenging technological applications. The outstanding electronic properties of diamond (high carriers mobility, saturation velocity, breakdown voltage, thermal conductivity), combined with its bio-compatibility, radiation hardness and optical transparency have led to the development of solid state devices for applications ranging from electronic devices [1-2] to radiation detectors [3-4] and devices for quantum technologies [5-7].
Together with the steady progresses in the development of efficient techniques for the electronic doping of diamond devices by homoepitaxial growth [7,8] or ion implantation [9-11], the fabrication of all-carbon devices by means of the local graphitization of its lattice upon laser irradiation [12,13] or MeV ion implantation [14,15] has been extensively explored. The latter technique consists of the selective conversion of a diamond volume to a graphitic phase upon the introduction of radiation damage produced by MeV or keV ion beams (typically focused to a micrometer spot size). In this way, it enables the direct fabrication of electrodes embedded in insulating diamond in arbitrary geometries, and thus the current injection [16,17] in specific micrometer-sized regions of the diamond bulk.
In particular, the Deep Ion Beam Lithography (DIBL) technique has been exploited to fabricate radiation detectors [18,19], cellular biosensors [20], waveguides [21], photonic structures [22], mechanical resonators [23], IR emitters [24] and more recently electrically-stimulated single-photon emitting devices [10,25]. The latter application relied on the injection of an electrical current in a diamond gap region comprised between micrometer-spaced graphitic electrodes, which was exploited to stimulate electroluminescence from color centers. These graphite-diamond-graphite junction structures exhibited peculiar electrical characteristics, in which an abrupt transition to a high-current regime

was observed at voltages above a critical threshold [17,25]. A preliminary interpretation of this phenomenon was based on Space Charge Limited Current (SCLC) and Poole-Frenkel (PF) conduction mechanisms [17], relying on carriers trapping/detrapping phenomena at localized defects. A more extensive study is required to qualify the nature and the effect of these traps, and to evaluate whether their origin is associated with the introduction of lattice damage as a side effect of the ion-beam-fabrication process. This investigation would enable to assess the perspectives and the limitations of DIBL for the development of future devices for quantum technologies (e.g.: electrically stimulated single photon sources), in which an extreme level of control on the material defectiveness is mandatory.
To these scopes, in this work a systematic investigation of the properties of a device consisting of a graphite-diamond-graphite junction realized with sub-superficial electrodes is performed as a function of temperature. The device under test is the same that was previously employed for the study of the electrical control of the charge state of nitrogen-vacancy complexes [17], where a preliminary (i.e. temperature-independent) investigation of the main features of charge transport was conducted.

2. Experimental

2.1 Sample fabrication

The device under study has undergone a preliminary electrical characterization, which is discussed in ref. [17]. To summarize, the sample was based on a 3×3×0.3 mm^3 single-crystal CVD IIa diamond substrate produced by ElementSix with nominal concentrations of substitutional nitrogen and boron of <1 ppm and <0.05 ppm, respectively. Two sub-superficial graphitic micro-electrodes were fabricated by raster-scanning a focused ∅~5 µm 6 MeV C^{3+} beam along linear paths at a fluence of ~4×10^{16} cm^{-2}. The chosen implantation fluence allowed to overcome the graphitization threshold (9×10^{22} vacancies cm^{-3} [26]) at the end of the ions range (**Figure 1a)**, i.e. ~2.7 µm below the sample surface according to SRIM Monte Carlo simulations [27] performed in "Detailed damage calculation" mode assuming a displacement energy value of 50 eV [28]. The sample was then annealed at 1000 °C in vacuum for 2 hours to achieve a conversion of the amorphized layer to a graphitic phase. The density of vacancies introduced in the inter-electrode gap by the implantation of stray ions, which can be assumed to be roughly constant in the whole active region of the device, was estimated as ~1×10^{22} cm^{-3}. While such density was significantly reduced by the recovery of the material upon thermal treatment [29], as reported in previous works [30] a complete recovery of the lattice structure in the inter-electrode gap cannot be assumed even for regions damaged below the critical amorphization threshold. Therefore, a residual amount of radiation damage and defects has to be considered. The sample was then treated in oxygen plasma (20 sccm O_2 flux, 30 W RF power, 2.5×10^{-2} mbar pressure, 30 min) to remove any residual surface conductivity resulting from the graphitization or contamination during the thermal treatment. The outer endpoints of the micro-channels were then milled by a 30 keV Ga^+ focused ion beam (FIB), to expose them to external electrical connections (**Figure 1c**), which were provided by the subsequent deposition of 70 nm thick Ag contacts through a stencil mask. The fabrication process resulted in two ~15 µm wide and ~100 µm long graphitic electrodes, spaced by a d ~ 9 µm gap (**Figure 1b**).

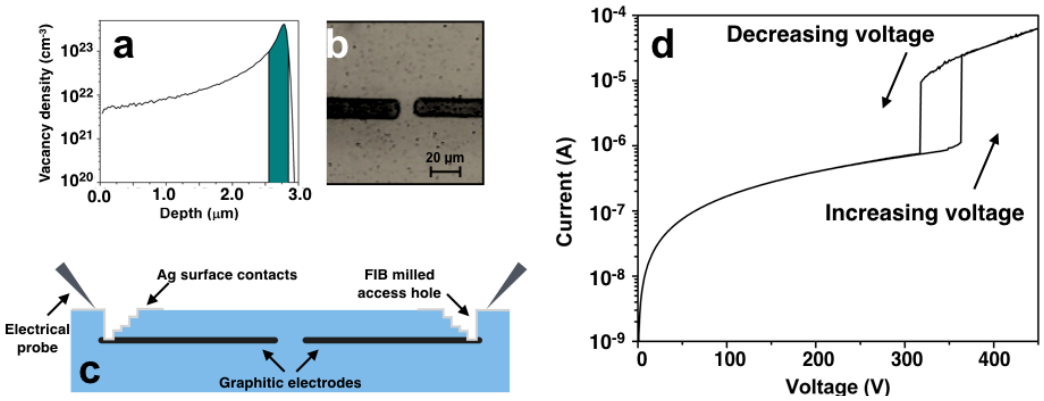

Figure 1: Fabrication of the diamond device with buried graphitic electrodes. **a)** Vacancy-density depth profile induced by 6 MeV C ions in diamond at an implantation fluence of 4×10^{16} cm^{-2}, as resulting from SRIM Monte Carlo simulations [27]. The region where the vacancy density exceeds the graphitization threshold is highlighted in green. **b)** Optical micrograph of the device. **c)** Schematic cross section of the device. The FIB-milled endpoints of the graphitic electrodes are exposed to Ag contact deposition, thus enabling the electrical characterization with two electrical microprobes. **d)** Typical room-temperature current voltage curve acquired from the device.

2.2 Electrical characterization

The electrical characterization of the device was performed in dark conditions at increasing temperatures in the 298-389 K range (3 K accuracy). The measurements were performed using a custom setup consisting of two

microprobes controlled by a set of micro-manipulators operating in a vacuum chamber (2×10^{-5} mbar pressure). The microprobes were connected through suitably shielded feedthroughs to a Keithley 6487 picoammeter, which was used to acquire current-voltage characteristics in a two-terminal configuration in the 0-450 V range with a bias step of 1 V.

3. Results

3.1 Electrical characterization at room temperature

The current-voltage characteristic of the device at room temperature (298 K) in the 0-450 V range is displayed in **Figure 1**. The $I(V)$ curve exhibits an ohmic trend at voltages up to ~350 V, where a deviation from the linear dependence is observed. When the bias reaches a critical threshold voltage $V_C \sim 365$ V, the junction exhibits an abrupt transition to a high-current regime. At voltages higher than V_C, the current follows a super-linear increase as a function of the applied bias.

When the applied bias is subsequently decreased back to zero, the $I(V)$ curve exhibits a hysteretic behavior, as the junction remains in the high-current regime until the applied voltage is reduced below a threshold value of $V_H \sim 310$ V, where an abrupt reversion to the ohmic regime is observed. The $I(V)$ features displayed in **Figure 1** are qualitatively consistent (i.e. despite differences in the electrodes geometries and the structural properties of the specific diamond susbtrates) with previous results obtained on the same sample [17], as well as in similar devices fabricated by C and He MeV implantation [31]. In the ohmic regime, the electrical conduction is dominated by electron transport in the inter-electrode gap, as resulting from previous findings on the stabilization of the negative charge state of optically-active nitrogen-vacancy defects at increasing bias in the same device [17], as well as from "Ion Beam Induced Charge" (IBIC) measurements [26].

The $I(V)$ curve in the high-current regime is compatible with a Poole-Frenkel conduction mechanism [32,33]. According to this model, the electrical conduction is dominated by the thermally-induced electron emission from traps into the conduction band under the effect of the strong applied electric field [34]. In this regime, the junction exhibits an intense electroluminescence from optically-active defects in the inter-electrode diamond gap, consistently with what is reported previous works [17,25,31].

The transition from ohmic to Poole-Frenkel conduction is very abrupt, as no evidence of a progressive variation in the measured current across the step is apparent, even by refining the voltage sampling to 0.1 V intervals. Such transition was interpreted in the previous works in terms of space-charge-limited current (SCLC), i.e. to an abrupt current increase associated with the progressive filling of electron traps upon the injection of electrons from the ohmic contacts [17]. According to this interpretation, the current transition at the critical threshold voltage V_C is due to the presence of charged traps in the diamond region, building up a screening electric field which prevents the injection of additional electrons at the cathode at $V< V_C$ [33]. The transition therefore occurs when the applied bias is high enough to overcome the above-mentioned field, thus enabling the injection of a high current in the diamond region of the junction. The steepness of the transition indicates that the trap density N_C is significantly higher than the density of electrons in the conduction band at $V<V_C$ [33]. It is worth noting that the observation of an hysteresis in the $I(V)$ curve suggests a small electron detrapping rate, and thus further supports our interpretation in terms of the SCLC model.

In particularly, as this investigation explores the opposite biasing polarity with respect to what reported in a previously published study on the same device [17], it is worth noting that the voltage transition occurs here at a slightly higher value of V_C (to be compared to ~300V in [17]). Furthermore, it is also worth mentioning that the values of V_C and V_H exhibited good reproducibility, with minimal variations (i.e. ~5 V) under repeated measurements in the same experimental conditions. Apart from these slight variations, the overall trend of the $I(V)$ characteristic was fully reproducible under multiple voltage cycles. These observations, consistently with our interpretation of trapping/detrapping-related effects in the electrical conduction, indicate that occasional variations in the trapped electrons in the trapped charge density in the inter-electrodes gap (i.e., the occurring of "memory effects" in the diamond device [35]) might determine small fluctuations to the value of V_C from cycle to cycle.

3.2 Temperature-dependent current-voltage characteristics

Ohmic conduction regime. Current-voltage characteristics in the same bias range were acquired at increasing temperatures from 320 K to 389 K, as indicated in **Figure 2a**, together with the room-temperature (298 K) characteristic.

In the ohmic region of the $I(V)$ curves, a progressive current increase is observed at increasing temperatures. Such temperature dependence of the conductance value can be written as

$$S(T)=K\,\mu_n(T)\,n(T)\,, \qquad (1)$$

where K is a proportionality factor including all the geometrical and temperature-independent parameters, μ_n is the electron mobility and the n is the electron density in conduction band. Eq. (1) can be further modified by considering the expression of n, under the assumption that the ohmic conduction arises from the thermal ionization of a monoenergetic donor distribution:

$$n = (N_C(T)\,N_D)^{1/2}\,e^{-E/k_BT} \propto T^{3/4}\,e^{-E_O/k_BT}\,. \qquad (2)$$

where k_B is the Boltzmann constant, $N_C \propto T^{3/2}$ is the effective density of states in the conduction band, N_D is the donor concentration, and E_O is the activation energy of the donor level responsible for the ohmic conduction.
Eq. (1) can be therefore rewritten as:

$$S(T) = K' \mu_n(\mathrm{T})\, T^{3/4}\ e^{-E_o/k_B T}, \qquad (3)$$

where again K' includes the product of all the temperature-independent parameters.
Figure 3a reports the Arrhenius plot that linearizes Eq. (3) as $[\ln(R) + 3/4 \ln T + \ln \mu_n]$ vs $(k_B T)^{-1}$, where R is the electrical resistance extracted from each $I(V)$ curve shown in **Figure 2a** from a linear fitting procedure in the 0-20 V range. The choice of this range was arbitrary, as the slope of the I(V) curves did not exhibit significant variations over the whole range of voltages in which the ohmic conduction regime was observed. The temperature-dependent values of the electron mobility were taken from ref. [36]. The slope of the linear fit in **Figure 3a** yields the activation energy of the relevant donor level, as E_O = (0.217 ± 0.002) eV. The very small relative uncertainty (~1%) associated with the activation energy is likely to be due to an underestimation arising from the fact that a fitting procedure was performed on a single dataset constituted of a large number of experimental data exhibiting a strong compatibility with the expected linear trend. Similar considerations can be made also for the ε_r, $q\Phi_t$, ΔE_t, N_t parameters discussed in the remainder of the text.
This value is in good agreement with the activation energies reported for donor levels associated with nitrogen impurities in single-crystal (0.22-0.28 eV [9]) and ultra-nanocrystalline diamond samples (0.13-0.22 eV) [37], where a n-type conduction was observed, as well as with the energy difference from the conduction band (0.2 eV) of the negative charge state of the A center in diamond (i.e., a nearest-neighbor pair of substitutional nitrogen atoms), as evaluated from density functional calculations [38]. These findings support *a posteriori* our initial assumption based on n-type conduction.

Electrical conduction in high-current regime. In high-current regime (i.e., at $V > V_C$), the $I(V)$ curves are satisfactorily described by the Poole-Frenkel conduction mechanism. Such regime is modeled by the following relation [34], that provides a mathematical generalization of the $i \sim V \sinh(V^{1/2})$ relation adopted in previous works [17,25]:

$$J = q\, \mu_n N_c\, \mathscr{E} \exp\{-q/(k_B T)\, [\phi_T - (q\, \mathscr{E} / \pi\, \varepsilon_0\, \varepsilon_r)^{1/2}]\} \qquad (4)$$

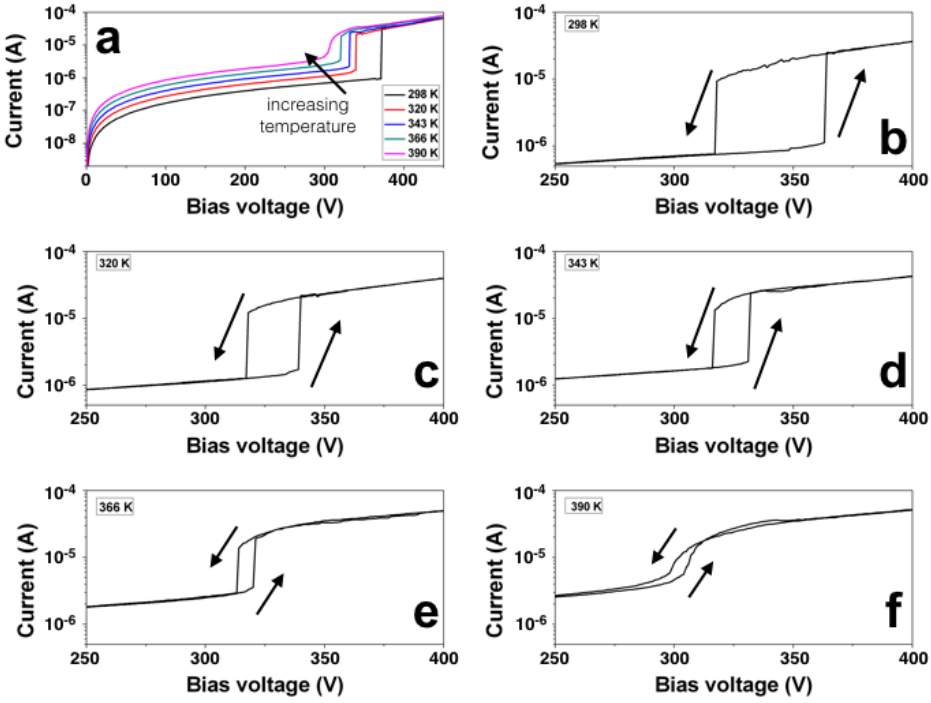

Figure 2: $I(V)$ curves of the graphite-diamond-graphite junction acquired at increasing temperatures. **a)** $I(V)$ curves in the 298-389 K range in semilogarithmic scale acquired at increasing voltage (1 V bias step). A zoom-in of the behavior of the $I(V)$ curves in the region around the transition edge to/from high-current regime is reported separately for each temperature in the following figures: **b)** 298 K, **c)** 320 K, **d)** 343 K, **e)** 366 K, and **f)** 389 K.

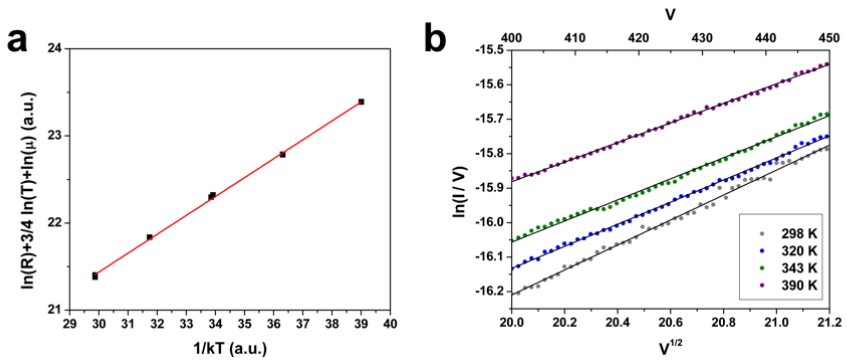

Figure 3: **a)** Arrhenius plot of $[\ln(K') + \ln(R(T)) + 3/4\ \ln(T) + \ln(\mu_n(T)]$ vs $(1/k_BT)$, as evaluated from the dependence of the conductance from temperature in the 0-20 V bias range. A linear fit (red solid line) yields the relevant donor trap as $\Delta E_O = (0.217 \pm 0.002$ eV. b) Plots linearizing the Poole-Frenkel trends of the $I(V)$ curves at applied bias above the critical voltage V_C, at various temperature. The linear fits (continuous lines) yield the dielectric constant of ion implanted diamond at different temperatures.

where J is the current density flowing in the active section of the inter-electrode gap region, which was estimated as $A = 4.5\times10^{-7}$ cm^2 from the optical measurement of the electrodes width and the SRIM-simulated penetration depth of 6 MeV C in diamond; $q\phi_T$ is the difference between the energy level of the trap and the conduction band; $\mathscr{E}=V/d$ is the local electric field, which was assumed to be constant in the active region of the junction; N_C is the density of states in the conduction band; ε_0 and ε_r are the vacuum permittivity and the dielectric constant of the material, respectively.

In **Figure 3b**, the data obtained at applied bias above the critical voltage V_C (i.e. between 400 V and 450 V) are reported at temperatures of 298 K, 320 K, 343 K and 389 K. The data acquired at 366 K were disregarded due to thermal instabilities occurred during the measurement in the high-current regime. The plotted quantities linearize Eq. (4), whereby the linear coefficient value is given by:

$$b = q/(k_BT)\ (q/(d\ \pi\ \varepsilon_0\ \varepsilon_r)^{1/2} \qquad (5)$$

From Eq. (5) it is possible to evaluate the relative dielectric constant ε_r at each temperature. **Table 1** summarizes the quantities evaluated from the linear fitting of the data reported in **Figure 3b**. The uncertainty on the value of the dielectric constant was estimated assuming a 1% accuracy (significantly affected by thermal fluctuations) in the measurement of the electrical current. The ε_r values determined at each operating temperature are not strictly compatible, most likely due to an underestimation of the relative uncertainties, and do not exhibit a clear trend as a function of temperature. Nonetheless, the weighted average value extracted from the measurement, $<\varepsilon_r> = 7.6 \pm 0.3$, reveals a ~35% increase with respect to the corresponding value for pristine diamond, i.e. $\varepsilon_r = 5.7$. To the best of the authors' knowledge, this result represents the first report on the effects of ion implantation on the dc dielectric constant in high-quality single-crystal diamond substrates, and it is in qualitative agreement with the increasing trend reported in previous studies on the refractive index (and thus in the ac dielectric constant) of diamond as a function of induced structural damage [39,40]. This can be explained on the basis of the increase in the material polarizability induced by the breaking of the covalent sp^3 bonds of diamond in favour of the formation of more polarizable defective complexes, but it is worth noting that in the measurements a non-negligible role in determining the dielectric response of the defective material is played by the space-charge polarization associated with the presence of a moderate density of charged defects in the active region of the junction, thus preventing a further quantitative comparison with previous results obtained for ac fields.

T [K]	b	ε_r
298	0.362 ± 0.004	7.43 ± 0.11
320	0.320 ± 0.002	8.19 ± 0.09
343	0.306 ± 0.003	7.85 ± 0.10
389	0.284 ± 0.002	7.05 ± 0.08

Table 1. Linear coefficients b of the best fit of the curves in Figure 3b and the corresponding value of the relative electrical permittivity ε_r as a function of temperature.

Voltage-dependent current-temperature characteristics. The variation of the current at increasing temperatures in the 305-400 K range was investigated while holding a fixed applied bias. Current-temperature characteristics $I(T)$ acquired at 150 V, 300 V and 350 V are displayed in **Figure 4**. The black dots superimposed to the $I(T)$ curves represent the data extracted from the previously reported $I(V)$ curves at the corresponding applied bias and temperature, exhibiting a satisfactory consistency between the two datasets.

At an applied bias of 150 V (see **Figure 4a**), the junction is in an ohmic conduction regime, and the current exponentially increases as a function of temperature, according to the typical trend observed in semiconductors. At 300 V bias (see **Figure 4b**), i.e. just below the critical voltage V_C in the whole considered temperature range, a progressive transition to the high-current regime occurs at increasing temperatures. This result is consistent with the previously-reported decreasing trend of V_C at increasing temperatures. In other terms, if a realistic non-monoenergetic distribution of defect-related levels in the band-gap is considered, our observation is consistent with the fact that at increasing temperatures a large fraction of defects act as electrically active dopants rather than charge traps.

At a bias voltage of 350 V (see **Figure 4c**), the junction operates in PF conduction regime over the whole temperature range under investigation, as confirmed by the data reported in **Figure 2**. Therefore, additional information on the relevant trap level $q\phi_T$ can be extracted according to Eq. (4). The data reported in **Figure 4c** are linearized by a $[\ln(I/V) - 3/2 \ln(T) - \ln(\mu(T))]$ vs $[1/(k_B T)]$ trend, in which the temperature dependence of μ_n and N_C can be made explicit in the same way as reported in Eq. (3), and whose corresponding linear coefficient is given by the following expression:

$$d = q\phi_T - q\,[q\,V / (d\,\pi\,\varepsilon_0\,\varepsilon_r)]^{1/2} \qquad (6)$$

The linearized $I(T)$ curve is reported in **Figure 4d** in the 340-400 K range. The fitting procedure (red line) yields a linear coefficient value of $d = -(0.0961 \pm 0.0004)$ eV. According to Eq. (6), this value corresponds to a trap level energy of $q\phi_T = (0.278 \pm 0.001)$ eV.
This value is again comparable with the activation energy of nitrogen-related defects in diamond [37] and with the energy difference from the conduction band (0.2 eV) of the negative charge state of the A-center [38], and is therefore close to the energy E_O related to the relevant donor responsible for ohmic conduction, so that an identification of the same defect as the main contributor to both current regimes is plausible.

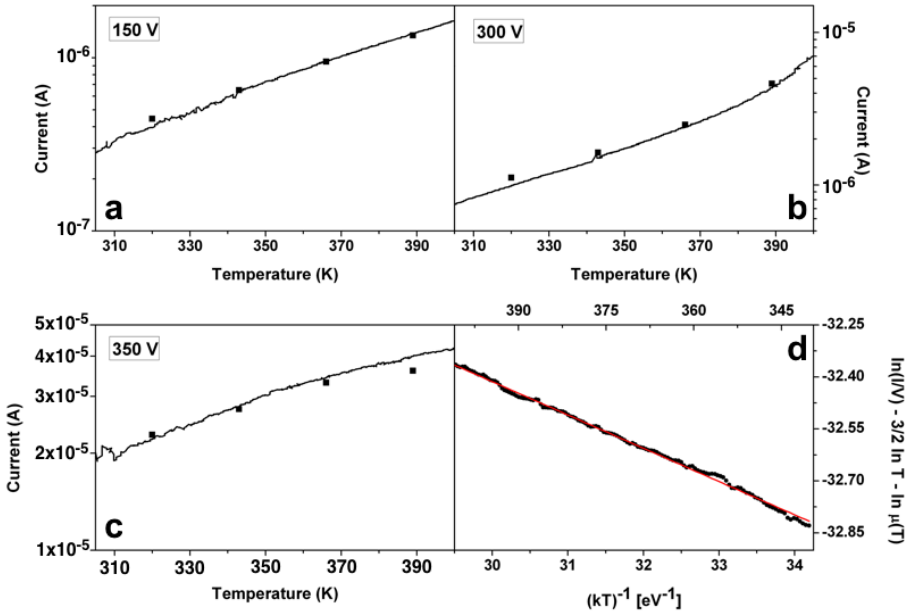

Figure 4: $I(T)$ curves (black line) acquired at a fixed bias voltage of **a)** 150 V, **b)** 300 V and **c)** 350 V. The square dots indicate the $I(V,T)$ data extracted from the $I(V)$ curves reported in **Figure 2**. **d)** Arrhenius plot linearizing the temperature-dependence of PF conduction. The best linear fit (red line) is superimposed to the experimental data.

Transition to the high-current regime. With regards to the transition to the high-current regime, as previously mentioned the critical voltage V_C shifts towards lower values at increasing temperatures, as the current responsible of the trap-filling process increases (see **Figure 2**). This behavior is in agreement with the qualitative model proposed by A. Rose in 1955 to model SCLC effects [32]. Concurrently, the bias voltage V_H at which the junction reverts back to the low-

current regime at decreasing biases exhibits a less pronounced decrease at increasing temperatures. As a consequence, the amplitude of the current hysteresis loop decreases from V_C-V_H ~ 100 V at room temperature to V_C-V_H ~ 10 V at 389 K. This effect is regarded as the result of an enhanced electron detrapping process, which is promoted by the increase in the substrate temperature. Moreover, the temperature increase smoothens the transition to high-current regime. In the 298–366 K temperature range, the transition is still sharp and no intermediate current values are measured between the low- and high-current regimes in the adopted experimental configuration. However, the departure of the $I(V)$ curves from the linear trend as the voltage approaches the critical value V_C becomes more apparent at increasing temperatures. The SCLC model allowed to estimate the energy difference (under the basic assumption of a monoenergetic electron trap distribution) ΔE_t between the conduction band and the relevant trap level, which is primarily responsible for the space charge build-up leading to the transition to the PF regime. By adopting the same procedure reported in [17], and considering the physical parameters reported in **Table 2** as well as the value of ε_r = 7.60 determined from the PF conduction regime, the position corresponding to this trap level was evaluated for each $I(V)$ curve acquired in the 298-389 K range. From the analysis, a value at room temperature of ΔE_t = (0.569±0.009) eV was derived, in excellent agreement with the value of (0.56 eV) previously determined on the same device [17].

The fact that the values of ΔE_t and $q\phi_T$ evaluated respectively from the SCLC and PF models are not compatible should not come as a surprise, as these conduction mechanisms are likely related to different (effective) energy levels in the band gap, the latter being too close to the conduction band to play a major role in the space charge build-up at room temperature.
Indeed, it is worth noting that at increasing temperatures the energy difference ΔE_t steadily increases up to a value of 0.68 eV at 389 K. Such effect could be explained by considering that the trap energy distribution in the band gap is unlikely to be mononergetic, and that ΔE_t should be regarded as an effective value resulting from the contribution of several defect types such as vacancies and NV centers [17]. The detrapping rate from the energy levels closer to the conduction band, including possibly those at $q\phi_T$ = 0.278 eV, is therefore increased at higher temperatures, so that the space charge build-up is limited to deeper traps in the band gap. This interpretation is also consistent with the steady decrease of the threshold voltage V_C at increasing temperatures, as the net space-charge to be overcome by the applied voltage is concurrently decreased. This effect is reflected in a steady decrease in the estimated net density of effective traps N_t, from a value of (3.79 ± 0.02)×10^{15} cm^{-3} at room temperature to (3.16±0.02)×10^{15} cm^{-3} at 389 K.

Symbol	Value at 298 K	Value at 320 K	Value at 343 K	Value at 389 K	Type of quantity
V_C [V]	365	339	331	320	Measured
V_{tr} [V]	350	333	325	282	Measured
N_t [cm^{-3}]	(3.79 ± 0.02)×10^{-15}	(3.52±0.02)×10^{-15}	(3.44±0.02)×10^{-15}	(3.16±0.02)×10^{-15}	Evaluated from $V_c = q\ N_t\ d^2 / (2\ \varepsilon_0\ \varepsilon_r)$ [33]
R [Ω]	7.0×10^8	4.2×10^8	2.7×10^8	1.3×10^8	Measured
μ_n [$cm^2\ V^{-1}\ s^{-1}$]	2870	2460	2231	1751	From literature [36]
n_0 [cm^{-3}]	6.2×10^9	1.2×10^{10}	2.0×10^{10}	5.7×10^{10}	Evaluated from $R^{-1}=q\ \mu_n\ n_0\ A\ d^{-1}$
N_C [cm^{-3}]	(1.0±0.2)×10^{20}	(1.1±0.3)×10^{20}	(1.2±0.3)×10^{20}	(1.5±0.4)×10^{20}	From literature (298 K); propagated through power law
θ [ ]	(3.04 ± 0.02)×10^{-6}	(6.22 ± 0.04)×10^{-6}	(1.074 ± 0.007)×10^{-5}	(3.44 ± 0.02) ×10^{-5}	Evaluated from $V_{tr} = 8/9\cdot(q\ n_0\ d^2)/(\varepsilon_0\ \varepsilon_r\ \theta)$ [34]
ΔE_t [eV]	0.569±0.009	0.596±0.007	0.63±0.01	0.68±0.01	Evaluted from $\theta = N_c/2/N_t\cdot\exp(-\Delta E_t/k_BT$ [33,34]

Table 2: List of values adopted for the calculation of the dominant electron trap energy level, according to the space-charge-limited current theory.

Conclusions

In this work we presented and analyzed the current-voltage characteristics acquired at variable temperature from a graphite-diamond-graphite junction based on sub-superficial micrometer-spaced electrodes.

At room temperature, the current flowing in the active region of the junction (i.e. the diamond region between the graphitic electrodes) exhibits an ohmic conduction trend dominated by a donor level with E_O = (0.217 ± 0.002) eV, which is compatible with previously reported results on nitrogen-related defects in diamond (e.g. the A center [9,36]). An abrupt transition to a high-current regime is then observed above a critical threshold voltage V_C. The $I(V)$ curve obtained at decreasing applied bias displays an hysteretic behavior which is ascribed to the presence of carriers trapped at deep energy levels in the band gap.

At increasing temperatures, this effect is mitigated by a steady decrease in the value of V_C and in the amplitude of the current hysteresis. The transition to the high-current regime is therefore interpreted in terms of the SCLC mechanism due to the formation of a space charge upon carriers trapping. Such interpretation is consistent with a decrease in the space charge density at increasing temperatures as a consequence of the reduction of the detrapping characteristic times of the energy levels closer to the conduction band.

The electrical conduction in high-current regime is suitably described in terms of the PF mechanism. From the fitting of the experimental data, the effective energy position of the level responsible for the electrical conduction was determined to be $q\phi_T$ = (0.268 ± 0.001) eV. This value is compatible with the negative charge state of the A-center in diamond [9,37], and a possible identification with the relevant defect responsible for the ohmic conduction regime is plausible.

The results obtained in this work provide a deeper insight in the electrical properties of graphite-diamond-graphite junctions for applications in opto-electronics. In particular, the temperature-dependent analysis allowed to extract information on the effective trap energy levels relevant to the above-mentioned conduction mechanisms. Furthermore, the fitting of the experimental data with the PF model enabled to estimate the value of the dc dielectric constant of implanted diamond as $< \varepsilon_r >$ = 7.60 ± 0.05 for a diamond subjected to a damage density of ~1×10^{22} cm^{-3} and subsequently annealed at 950° C for two hours. The ~35% increase in the value of the dielectric constant with respect to that of pristine diamond was qualitatively ascribed to both the damage-induced increase of the polarizability of the material and the presence of a space distribution of charged defects in the active volume of the device.

The conduction mechanisms identified in the device under investigation are deeply related to the presence of electrically-active nitrogen-related complexes, either native or associated with the ion implantation process. However, since the availability of arbitrary electrodes geometry is an appealing perspective to electrically address the optical emission of diamond color centers, it will be of significant interest to assess whether the same conduction mechanisms observed in this work will still control the electrical properties of intrinsic substrates with significantly higher elemental purity. Although this goes beyond the scopes of the present work, it is worth remarking that a significant decrease of the threshold voltage V_C should be expected for lower defects concentrations, i.e. in "electronic grade" diamond. Additionally, a small enough trap density could result in the absence of a SCLC conduction in the active region of the device. To further investigate this latter point, in addition to adopting samples characterized by an extremely low concentration of native defects, minimizing radiation damage in the active volume of the device will be necessary. This goal can be achieved by the fabrication of graphitic electrodes through micrometer-sized implantation masks, which would prevent the introduction of undesired radiation-induced defects in the inter-electrode gap [41], or alternatively, through the fabrication of charge-injecting electrodes by means of laser-induced graphitization techniques [42,43].
In principle, a smaller defects concentration in the active region of such devices could lead to a lower critical voltage V_C required to stimulate electroluminescent emission from color centers, as well as to a more efficient control of the charge state of individual defects at low applied biases [17].

Acknowledgements

This research was supported under the following schemes: "DIESIS" project funded by the Italian National Institute of Nuclear Physics (INFN) - CSN5 within the "Young research grant" scheme; "Diamond Microfabrication" experiment at the "Nanofacility Piemonte" laboratory of INRiM, supported by the "Compagnia di San Paolo" Foundation.

References

[1] R. Nemanich, J. Carlisle, J.A.Hirata, K. Haenen, *CVD diamond—Research, applications, and challenges*, MRS Bulletin 39 (2014) 490. doi: 10.1557/mrs.2014.97.

[2] C.E. Nebel, *Electronic properties of CVD diamond*, Semiconductor Science and Technology 18 (2003) S1. doi: 10.1088/0268-1242/18/3/301.

[3] The RD42-Collaboration, *A 3D diamond detector for particle tracking*, Nucl. Instr. Meth. A 824 (2016) 402. doi: 10.1016/j.nima.2015.09.079.

[4] N. Skukan, V. Grilj, I. Sudić, M. Pomorski, W. Kada, T. Makino, Y. Kambayashi, Y. Andoh, S. Onoda, S. Sato, T. Ohshima, T. Kamiya, M. Jakšić, *Charge multiplication effects in thin diamond films*, Applied Physics Letters 109, 043502 (2016). doi:

10.1063/1.4959863.

[5] J.B.S. Abraham, B. A. Aguirre, J.L. Pacheco, G.Vizkelethy, E. Bielejec, *Fabrication and characteriztion of a co-planar detector in diamond for low energy single ion implantation*, Applied Physics Letters 109 (2016) 063502. doi: 10.1063/1.4960968.

[6] E. Bourgeois, A. Jarmola, P. Siyushev, M. Gulka, J. Hruby, F. Jelezko, D. Budker, M. Nesladek, *Photoelectric detection of electron spin resonance of nitrogen-vacancy centres in diamond*, Nat. Commun. 6 (2015) 8577. doi: 10.1038/ncomms9577.

[7] N. Mizuochi, T. Makino, H. Kato, D. Takeuchi, M. Ogura, H. Okushi, M. Nothaft, P. Neumann, A. Gali, F. Jelezko, J. Wrachtrup, S. Yamasaki, *Electrically driven single-photon sourced at room temperature in diamond*, Nat. Photonics 6, 299 (2012). doi: 10.1038/nphoton.2012.75.

[8] S. Yamasaki, E. Gheeraert, Y. Koide, *Doping and interface of homoepitaxial diamond for electronic applications*, MRS Bulletin 39 (2014) 499. doi:10.1557/mrs.2014.100.

[9] J. F. Prins, *Nitrogen-related n-type conduction with low thermal activation in diamond*, Semicond. Sci. Technol. 16 (2001) L50. doi: 10.1088/0268-1242/16/9/102.

[10] A. Lohrmann, S. Pezzagna, I. Dobrinets, P. Spinicelli, V. Jacques, J.-F. Roch, J. Meijer, A.M. Zaitsev, *Diamond based light-emitting diode for visible single-photon emission at room temperature*, Appl. Phys. Lett. 99 (2011) 251106. doi: 10.1063/1.3670332.

[11] L. H. Willems van Beveren, R. Liu, H. Bowers, K. Ganesan, B. C. Johnson, J. C. McCallum, S. Prawer, *Optical and electronic properties of sub-surface conducting layers in diamond created by MeV B-implantation at elevated temperatures*, J. Appl. Phys. 119 (2016) 223902. doi:10.1063/1.4953583.

[12] A. Oh, B. Caylar, M. Pomorski, T. Wengler, *A novel detector with graphitic electrodes in CVD diamond*, Diamond and Related Materials 38, (2013) 9. doi:10.1016/j.diamond.2013.06.003.

[13] T. V. Kononenko, P. N. Dyachenko, and V. I. Konov, *Diamond photonic crystals for the IR spectral range*, Optics Letters 39 (2014) 6962. doi: 10.1364/OL.39.006962.

[14] R. Kalish, S. Prawer, *Graphitization of diamond by ion impact: Fundamentals and applications*, Nucl. Instr. and Meth. B 106 (1995) 492. doi: 10.1016/0168-583X(95)00758-X.

[15] R. Kalish; A. Reznik; K.W. Nugent, S. Prawer, *The nature of damage in ion-implanted and annealed diamond*, Nucl. Instrum. Methods Phys. Res. B 148 (1999) 626. doi:10.1016/S0168-583X(98)00857-X.

[16] A.A. Gippius, R.A. Khmelnitskiy, V.A. Dravin, S.D. Tkachenko, *Formation and characterization of graphitized layers in ion-implanted diamond*, Diamond Relat. Mater. 8 (1999) 1631. doi: 10.1016/S0925-9635(99)00047-3.

[17] J. Forneris, S. Ditalia Tchernij, A. Tengattini, E. Enrico, V. Grilj, N. Skukan, G. Amato, L. Boarino, M. Jakšić, P. Olivero, *Electrical control of deep NV centers in diamond by means of sub-superficial graphitic micro-electrodes*, Carbon 113 (2017) 76. doi: 10.1016/j.carbon.2016.11.031.

[18] J. Forneris, V. Grilj, M. Jakšić, P. Olivero, F. Picollo, N. Skukan, C. Verona, G. Verona-Rinati, E. Vittone, *Measurement and modelling of anomalous polarity pulses in a multi-electrode diamond detector*, EPL, 104 (2013) 28005. doi: 10.1209/0295-5075/104/28005.

[19] P.J. Sellin, A. Galbiati, *Performance of diamond x-ray sensor fabricated with metal-less graphitic contacts*, Appl. Phys. Lett. 87 (2005) 093502. doi: 10.1063/1.2035885.

[20] F. Picollo, A. Battiato , E. Carbone, L. Croin, E. Enrico, J. Forneris, S. Gosso, P. Olivero, A. Pasquarelli, V. Carabelli, *Development and characterization of a diamond-insulated graphitic multi electrode array realized with ion beam lithography*, Sensors 2015, 15, 515-528. doi:10.3390/s150100515.

[21] P. Olivero, S. Rubanov, P. Reichart, B.C. Gibson, S.T. Huntington, J. Rabeau, A.D. Greentree, J. Salzman, D. Moore, D.N. Jamieson, S. Prawer, *Ion-beam.assisted lift-off technique for three-dimensional micromachining of freestanding single-crystal diamond*, Adv. Mater. 17 (20) (2005) 2427. doi: 10.1002/adma.200500752.

[22] I. Bayn, B. Meyler, A. Lahav, J. Salzman, R. Kalish, B.A. Fairchild, S. Prawer, M. Barth, O. Benson, T. Wolf, P. Siyushev, F. Jelezko, J. Wrachtrup, *Processing of photonic crystal nanocavity for quantum information in diamond*, Diamond Relat. Mater. 20 (2011) 937. doi: 10.1016/j.diamond.2011.05.002.

[23] J.C. Lee, I. Aharonovich, A.P. Magyar, F. Rol, E.L. Hu, *Coupling of silicon-vacancy centers to a single crystal diamond cavity*, Opt. Expr. 20 (8) (2012) 8891. doi: 10.1364/OE.20.008891.

[24] M. Liao, S. Hishita, E. Watanabe, S. Koizumi, Y. Koide, *Suspended single-crystal diamond nanowires for high-performance nanoelectromechanical switches*, Adv. Mater. 22 (2010) 5393. doi: 10.1002/adma.201003074.

[25] J. Forneris, P. Traina, D. Gatto Monticone, G. Amato, L. Boarino, G. Brida, I.P. Degiovanni, E. Enrico, E. Moreva, V. Grilj, N. Skukan, M. Jaksic, M. Genovese, P. Olivero, , *Electrical stimulation of non-classical photon emission from diamond color centers by means of sub-superficial graphitic electrodes*, Scientific Reports 5 (2015) 15901. doi: 10.1038/srep15901.

[26] P. Olivero, J. Forneris, M. Jakšić, Ž. Pastuović, F. Picollo, N. Skukan, E. Vittone, *Focused ion beam fabrication and IBIC characterization of a diamond detector with buried electrodes*, Nuclear Instruments and Methods in Physics Research B 269 (2011) 2340 . doi: 10.1016/j.nimb.2011.02.021.

[27] J.F. Ziegler,M.D. Ziegler, J.O. Biersack, *SRIM—The stopping and range of ions in matter*, Nucl. Instrum. Meth. B 268 (2010) 1818. doi:10.1016/j.nimb.2010.02.091.

[28] D. Saada, J. Adler, R. Kalish, *Transformation of diamond (sp^3) to graphite (sp^2) bonds by ion-impact*, Int. J. Mod. Phys. C (1998) 61. doi: 10.1142/S0129183198000066.

[29] A.M. Zaitsev, *Optical Properties of Diamond*, Springer, New York, 2001.

[30] L. Allers, A. T. Collins, J. Hiscock, *The annealing of interstitial-related optical centres in type II natural and CVD diamond*, Diamond Relat. Mater. 7, 228–232 (1998). doi. 10.1016/S0925-9635(97)00161-1.

[31] J. Forneris, A. Battiato, D. Gatto Monticone, F. Picollo, G. Amato, L. Boarino, G. Brida, I. P. Degiovanni, E. Enrico, M. Genovese, E. Moreva, P. Traina, C. Verona, G. Verona Rinati, P. Olivero, *Electroluminescence from a diamond device with ion-beam-micromachined buried graphitic electrodes,* Nucl. Instrum. Meth. B 348 (2015) 187. doi: 10.1016/j.nimb.2014.12.036.

[32] A. Rose, *Space-charge-limited currents in solids*, Phys. Rev. 97 (1955) 1538. doi:10.1103/PhysRev.97.1538.

[33] M.A. Lampert, *Simplified theory of space-charge-limited currents in an insulator with traps*, Phys. Rev. 103 (1956) 1648. doi: 10.1103/PhysRev.103.1648.

[34] F.-C. Chiu, Adv. Mat. *A review on conduction mechanisms in dielectric films*, Sci. and Engineering (2014) 578168. doi: 10.1155/2014/578168.

[35] C. Manfredotti, A. Lo Giudice, E. Vittone, F. Fizzotti, Y. Garino, E. Pace, *Memory effects in CVD diamond*, Diamond & Related Materials 15 (2006) 1467. doi: 10.1016/j.diamond.2005.10.058.

[36] F. Nava, C. Canali, C. Jacoboni, L. Reggiani, S.F. Kozlov, *Electron effective masses and lattice scattering in natural diamond*, Solid State Commun. 33, (1980) 475. doi. 10.1016/0038-1098(80)90447-0.

[37] V.I. Polyakova, A.I. Rukovishnikova, N.M. Rossukanyia, V.G. Pereverzevb, S.M. Pimenovb, J.A. Carlislec, D.M. Gruenc, E.N. Loubnind, *Charge-based deep level transient spectroscopy of undoped and nitrogen-doped ultrananocrystalline diamond films*, Diamond and Related Materials 12 (2003) 1776. doi: 10.1016/S0925-9635(03)00203-6.

[38] J.P. Goss, P.R. Briddon, R. Jones, S. Sque, *Donor and acceptor states in diamond*, Diamond and Related Materials 13 (2004) 684. doi: 10.1016/j.diamond.2003.08.028.

[39] R. L. Hines, *Radiation damage of diamond by 20-keV carbon ions*, Phys. Rev. 138 (6A), A1747 (1965). doi: 10.1103/PhysRev.138.A1747.

[40] P. Olivero, S. Calusi, L. Giuntini, S. Lagomarsino, A. Lo Giudice, M. Massi, S. Sciortino, M. Vannoni, E. Vittone, *Controlled variation of the refractive index in ion-damaged diamond*, Diamond and Related Materials 19 (2010) 428. doi: 10.1016/j.diamond.2009.12.011.

[41] F. Picollo, A. Battiato, E. Bernardi, L. Boarino, E. Enrico, J. Forneris, D. Gatto Monticone, P. Olivero, *Realization of a diamond based high density multi electrode array by means of Deep Ion Beam Lithography*, Nucl. Instr. Meth. B 348 (2015) 199. doi: 10.1016/j.nimb.2014.11.119.

[42] S. Lagomarsino, M. Bellini, C. Corsi, F. Gorelli, G. Parrini, M. Santoro, S. Sciortino, *Three-dimensional diamond detectors: Charge collection efficency of gragphitic electrodes*, Applied Physics Letters 103, 233507 (2013). doi:10.1063/1.4839555.

[43] M. De Feudis, A.P. Caricato, G. Chiodini, M. Martino, E. Alemanno, G. Maruccio, A.G. Monteduro, P.M. Ossi, R. Perrino, S. Spagnolo, *Characterization of surface graphitic electrodes made by excimer laser on CVD diamond*, Diamond & Related Materials 65 (2016) 137. doi: 10.1016/j.diamond.2016.03.003.